Materials Chemistry and Physics 147 (2014) 649–660

Contents lists available at ScienceDirect

Materials Chemistry and Physics

journal homepage: www.elsevier.com/locate/matchemphys

A comprehensive study of soft magnetic materials based on FeSi spheres and polymeric resin modified by silica nanorods

M. Strečková [a, *], J. Füzer [b], L. Kobera [c], J. Brus [c], M. Fáberová [a], R. Bureš [a], P. Kollár [b], M. Lauda [b], Ľ. Medvecký [a], V. Girman [b], H. Hadraba [d], M. Bať ková [e], I. Bať ko [e]

[a] Institute of Materials Research, Slovak Academy of Sciences, Watsonova 47, 040 01 Košice, Slovak Republic
[b] Institute of Physics, Faculty of Science P. J. Šafárik University, Park Angelinum 9, 040 01 Košice, Slovak Republic
[c] Institute of Macromolecular Chemistry ASCR, Heyrovský sq. 2, 162 06 Prague 6, Czech Republic
[d] CEITEC IPM, Institute of Physics of Materials ASCR, Zizkova 513/22, 616 62 Brno, Czech Republic
[e] Institute of Experimental Physics, Slovak Academy of Sciences, Watsonova 47, 040 01 Košice, Slovak Republic

HIGHLIGHTS

- Soft magnetic composites are designed for electrotechnical applications.
- Electroinsulating layer consists of phenolic resin modified with silica nano-rods.
- NMR, FTIR and DSC analysis is used to characterize hybrid resin.
- Spherical Fe–Si particles covered by hybrid resin form a core–shell composite.
- Mechanical, electrical and magnetic properties are described in detail.

GRAPHICAL ABSTRACT

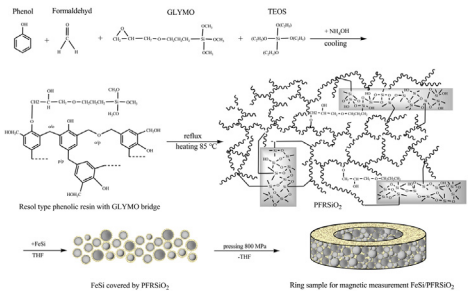

ARTICLE INFO

Article history:
Received 24 July 2013
Received in revised form
19 April 2014
Accepted 2 June 2014
Available online 21 June 2014

Keywords:
A. Composite materials
A. Magnetic materials
B. Chemical synthesis
C. Electron microscopy
D. Magnetic properties

ABSTRACT

A novel soft magnetic composite (SMC) based on spherical FeSi particles precisely covered by hybrid phenolic resin was designed. The hybrid resin including silica nano-rods chemically incorporated into the phenolic polymer matrix was prepared by the modified sol–gel method. A chemical bridge connecting silica nano-rods with the base polymeric net was verified by FTIR, ^{13}C and ^{29}Si NMR spectroscopy, whereas the shape and size of silica nano-rods were determined by TEM. It is shown that the modification of polymeric resin by silica nano-rods generally leads to the improved thermal and mechanical properties of the final samples. The hybrid resin serves as a perfect insulating coating deposited on FeSi particles and the core–shell particles can be further compacted by standard powder metallurgy methods in order to prepare final samples for mechanical, electric and magnetic testing. SEM images evidence negligible porosity, uniform distribution of the hybrid resin around FeSi particles, as well as, dimensional shape stability of the final samples after thermal treatment. The hardness, flexural strength and density of the final samples are comparable to the sintered SMCs, but they simultaneously exhibit much higher specific resistivity along with only slightly lower coercivity and permeability.

© 2014 Elsevier B.V. All rights reserved.

* Corresponding author. Tel.: +421 55 7922402; fax: +421 55 7922408.
E-mail address: mstreckova@imr.saske.sk (M. Strečková).

http://dx.doi.org/10.1016/j.matchemphys.2014.06.004
0254-0584/© 2014 Elsevier B.V. All rights reserved.

1. Introduction

The insulating soft magnetic composites (SMCs) are traditionally designed from magnetic metal powders, which are covered ideally by a very thin insulating layer [1]. The most important features of the insulating SMCs are low eddy current losses and relatively low total core losses at higher frequencies [2]. Moreover, the isotropic three-dimensional magnetic and electrical properties allow a flexible machine design and assembly what consequently leads to a substantial reduction in the overall weight and production cost of the final products. Nowadays, SMCs are very perspective materials for production of diverse electromagnetic devices such as rotors, stators, compressors, induction coil cores, actuators, electrical converters and other rotating devices [3–5]. SMCs allow building devices of more complex geometries with a lower price using environmentally-friendly techniques. A powder metallurgy (PM) technology is a common economic process for mass production of near-net-shape parts. The aim of PM technologies is to achieve SMCs with a high enough density and sufficiently stable mechanical properties, whereas an insulation layer between magnetic powder particles should ensure a high electrical resistivity minimizing the overall magnetic losses. The dielectric materials used for the insulation can be selected from organic polymeric resins [6], or inorganic materials such as metals, oxides, phosphates, or silicates [7–9]. Recently, Högänes Corporation has developed a high-purity FeSi powder, which is quite superior with respect to the pure iron powder as it provides optimal ground for a further development of SMCs [10]. It is a well known fact that silicon added to iron increases its resistivity, which consequently reduces power losses due to eddy currents. The silicon content of 3 wt % in FeSi alloy gives a specific resistivity of about 50 μΩ cm. The higher silicon content further increases the specific resistivity of the FeSi alloy, but it simultaneously decreases a magnetic induction and makes the material extremely brittle. The sintering of the FeSi alloy is carried out entirely in α phase leading to a formation of sizable ferrite grains, which promote low coercive force and high permeability [1]. Owing to the low coercivity and high resistivity, SMCs consisting of the FeSi particles covered by a thin electro-insulating layer could be applied for circuits subject to alternating or pulsed voltage (currents) with frequencies ranging from hundreds to several thousand hertz. The main disadvantage of those materials usually lies in their low mechanical strength, because these materials are not sintered during their preparation. Instead, the SMCs are cured under the curing schedule determined by the used insulating layer. The other disadvantage of the SMCs lies in a higher porosity, which is in general more conspicuous for the SMCs involving the organic binder [11]. The saturation induction of SMCs depends linearly on a density and hence, the increase in porosity leads to a subsequent increase of hysteresis losses due to a more restricted movement of magnetic domains [12].

The magnetic performance of SMCs can be basically tuned by selecting appropriate base ferromagnetic material and applying suitable insulating coating. Until now, the organic thermoset resins have turned out to be the most convenient insulating coatings for the base ferromagnetic materials [13–17]. To improve the mechanical hardness and flexural strength of the final SMCs, the organic polymers are usually modified with some inorganic filler. Reinforced polymer composites are prepared by an artificial incorporation of diverse inorganic additives (e.g. natural fibers, clays, silica, carbon nanorods or graphene) into the polymer matrix during its synthesis [18–20]. One should bear in mind that an incorporation of some inorganic fillers such as silica may cause the incompatibility between hydrophilic particles and hydrophobic polymer matrix in the processing of the hybrid inorganic–organic coating having some important consequences on the final material properties. In addition, SiO_2 particles have a tendency to agglomerate into bundles and unevenly distribute in the polymer matrix, which can be to a certain extent avoided using various coupling agents [21]. A coupling agent is a chemical substance, which serves for creating a chemical bridge between the inorganic additive and organic polymer matrix at the relevant interface [22]. For the particular case of the silica filler, the silane molecules with bifunctional groups may be used as suitable coupling agents providing a chemical bridge in between the inorganic additive and organic polymer matrix [23]. The resol-type phenolic resin is synthesized by the polycondensation reaction of phenol with formaldehyde that proceeds under the alkaline condition with the excess of formaldehyde reagent. The final product of this reaction is a rather complex network of the thermoset phenolic resin [24]. The combination of organic polymer matrix and the appropriate inorganic additive leads to the hybrid organic–inorganic coating with the improved physical, mechanical, and thermal properties [6]. It is quite well established that the sol–gel process provides the suitable method for the chemical incorporation of nano-sized particles into the polymer matrix [25]. The usual precursor for the creation of nano-silica particles inside the organic polymeric network is tetraethylorthosilicate as depicted in Scheme 1. The sol–gel process represents a very complex reaction affected by many variables such as the type of alkoxide, pH, amount of water, cosolvent, temperature, etc. Chiang et al. [25] have shown that the condensation reaction is faster than hydrolysis in the alkaline solution, which subsequently results in highly condensed species agglomerating into fine particles.

In the present work, the insulating layer of the designed SMCs is formed by the hybrid phenol–formaldehyde resin (PFR) modified by SiO_2 nano-particles hereafter abbreviated as PFRSiO_2. Using two different types of silanes, the hybrid polymers with the chemically incorporated SiO_2 nanoparticles of nano-rod shape were produced in situ within the polymer matrix. The chemical modification of polymer matrix by silica was confirmed by NMR and FTIR analysis. The thermal degradation of hybrid polymer was studied and the optimal curing schedule for the final FeSi/PFRSiO_2 samples was suggested. TEM, SEM and EDX analysis was performed in order to

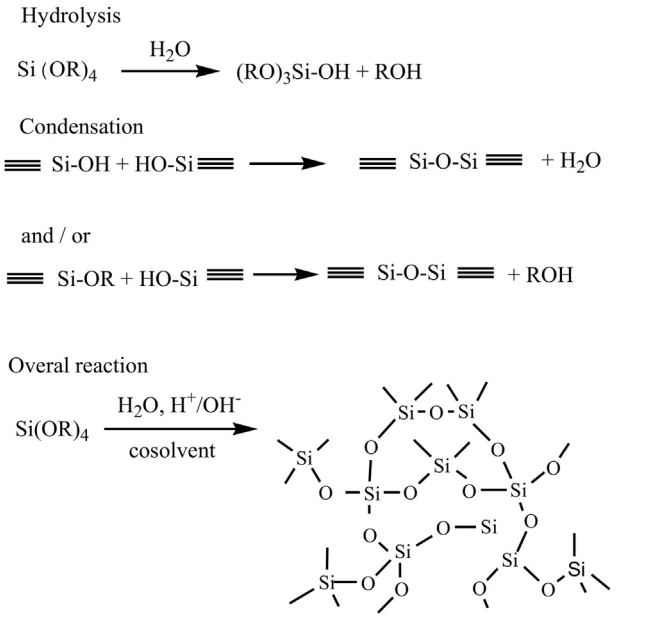

Scheme 1. Basic steps of a sol–gel process leading to a preparation of SiO_2 particles from the precursor tetraethylorthosilicate.

provide a detailed characterization of silica nanoparticles intercalated in the polymer matrix. The one-axis compaction of the insulated FeSi/PFRSiO$_2$ powder was employed for the preparation of the final samples used for further mechanical, electrical and magnetic tests. The interface between the polymeric coating and the FeSi powder was examined by AFM and the distribution of magnetic domains in the original FeSi powder by MFM. The base mechanical, electric and magnetic measurements of the prepared FeSi/PFRSiO$_2$ material were performed.

2. Experimental

2.1. Materials

The commercial powder of FeSi spherical particles with the granulometric fraction from 45 μm to 150 μm, which is distributed by Högänes Corporation [10], was used as the base ferromagnetic material. The chemical composition of FeSi was 97 wt% of Fe, 2.8 wt % of Si, 0.003 wt% of C, 0.04 wt% of O and 0.01 wt% of N. The other chemicals of analytical grade used for synthesis were obtained from Sigma–Aldrich without further purification. Phenol (Ph, 99%), formaldehyde (F, 37% aq.), ammonia (NH_3, 26% aq.), tetraethylorthosilicate (TEOS, 99%) and 3-glycidoxypropyltrimethoxysilane (GLYMO, 98%) were used for the synthesis of the pure PFR and the hybrid PFRSiO$_2$. The tetrahydrofuran (THF, 99.9%) and the absolute ethanol were used as the solvents.

2.2. Synthesis of PFRSiO$_2$

The synthesis of the pure PFR was performed according to the procedure as described in our previous work [6]. The preparation of the hybrid PFRSiO$_2$ polymer with the chemical incorporation of silica nano-rods is depicted on Scheme 2. The initial molar reaction ratio of Ph/F/NH_3/GLYMO/TEOS was 1.0/1.5/0.35/0.1/0.1. Phenol and formaldehyde were mixed in the round-bottomed flask until the complete dissolving of phenol was achieved. The predetermined amount of GLYMO was added to the prepared binary solution and mixed for 10 min. In the next step, TEOS was added to the ternary solution. NH_3 as a catalyst was added dropwise to the cooled mixture, what leads to the creation of white precipitate. The separation of water and organic phase was observed in the solution during 45 min refluxing at 80 °C. The water phase was removed by vacuum distillation for 45 min at 95 °C. PFRSiO$_2$ prepolymer is transparent with honey-like viscosity after the preparation. The amount of SiO_2 was determined by spectrophotometrically via Si–Mo–V complex as 0.52%.

2.3. Preparation of FeSi/PFRSiO$_2$ samples

The prepared hybrid PFRSiO$_2$ prepolymer is insoluble in the most of solvents, but it can be dissolved in THF. PFRSiO$_2$ was diluted approximately in 5 ml of THF and the appropriate amount of FeSi powder (cca. 20 g) was added into this clear solution. Suspension was mixed until the complete evaporation of solvent. The coated FeSi/PFRSiO$_2$ powder was compacted at 800 MPa to the three different shapes in order to obtain the final samples for the further analysis and testing. Vickers hardness test HV10 (STN-EN-ISO 6507-1 (42 0374), MPIF 43) and electrical resistivity tests were measured on the cylindrical shaped samples with dimensions of 10 × 3 mm ($d \times h$). The flexural strength (STN (42-0891-4), MPIF41) was detected on prism-shaped samples of dimensions 5 × 4 × 2 mm ($w \times h \times l$). Magnetic measurements were recorded on the toroid-

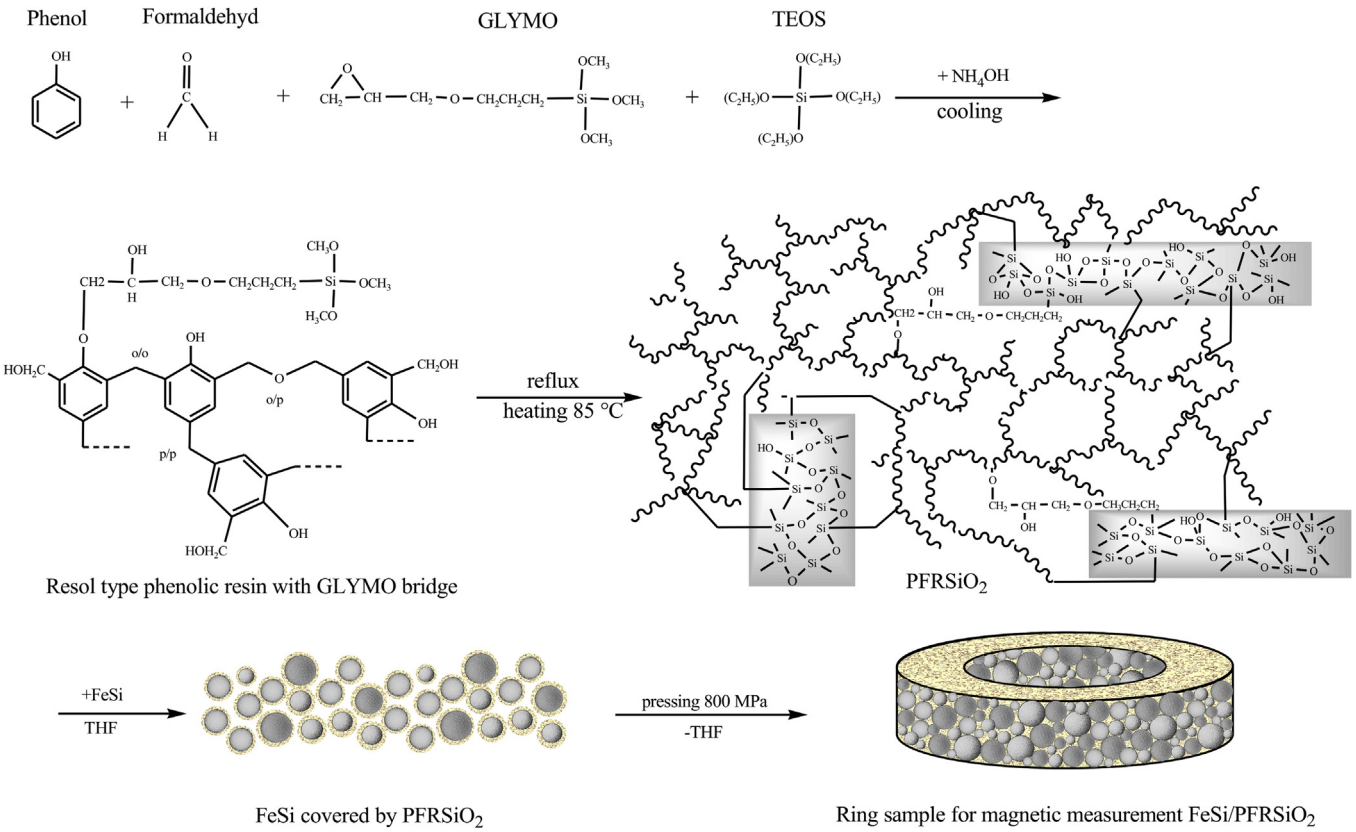

Scheme 2. A reaction scheme for a synthesis of the hybrid polymeric resin PFRSiO$_2$ and the basic steps of the preparation of the ring-shaped sample FeSi/PFRSiO$_2$ used for magnetic measurements.

shaped samples with the outer diameter of 24 mm, the inner diameter of 17 mm and the height of 2 mm. All prepared samples were thermally treated according to the curing schedule, which was suggested due to the thermal degradation of the hybrid resin (see Table 1). The density of each prepared sample was determined by the helium pycnometer (AccuPyc II 1340, Micromeritics) ($n = 15$).

2.4. Methods for characterization

All NMR spectra were measured at 11.7 T using a Bruker Avance 500 WB/US NMR spectrometer equipped with a double-resonance 4-mm MAS probehead. The ^{13}C CP/MAS NMR spectra were recorded at Larmor frequencies $\nu\ ^{13}C = 125.783$ MHz. Magic angle spinning (MAS) frequency of the sample was 11 kHz. The number of scans for the accumulation of ^{13}C CP/MAS NMR spectra was 4096 with repetition delay 4 s, and 1.5 ms spin lock. The isotropic chemical shift of ^{13}C scale was calibrated with glycine as an external standard (176.03 ppm to carbonyl signal). The ^{29}Si CP/MAS NMR spectra at $\nu\ ^{29}Si = 99.325$ MHz were acquired; spinning frequency was $\omega r/2\pi = 7$ kHz; contact time was 5 ms and number of scans was 13,312 with recycle delay 3 s. The spectra were referenced to M8Q8 (octamethylsilsesquioxane, the highest-field signal is set to −109.8 ppm). The strong heteronuclear dipolar couplings were eliminated by high-power dipolar decoupling during detection. Frictional heating during fast rotation of sample was taken into consideration. The temperature was calibrated using the $Pb(NO_3)_2$ sample at 308 K and the calibration procedure is described in literature [26].

Fourier transform infrared spectra (FTIR) were recorded by FTIR spectrophotometer (Shimadzu, IRAffinity, KBr pellets 1 mg sample + 300 mg KBr) before and after curing. The background originating from KBr pellet was subtracted from spectra. The average spectra were obtained after accumulation of 100 records with resolution of 2 cm^{-1} in the range from 4000 to 400 cm^{-1}. The thermal degradation of $PFRSiO_2$ was analyzed by differential scanning calorimeter (METTLER 2000 C). The samples were heated up to 700 °C in air at a heating rate of 10 °C min^{-1}.

The microstructure and morphology of all the samples were examined by the scanning electron microscope SEM (JEOL JSM-7000F) equipped with the energy dispersive X-ray analyzer (EDX) after the carbon coating. The polymer samples were ultramicrotomized with a diamond trimming knife (Leica EM UC7) at room temperature to give sections with a nominal thickness of 100 nm. The sections were transferred on carbon-coated 200-mesh Cu grids. The bright-field TEM images were explored at 200 kV by the transmission electron microscopy TEM (JEOL 2100F).

AFM-MFM measurements was used in order to observe topography and magnetic domains of $FeSi/SiO_2$ sample on Dimension Icon® Atomic Force Microscope made by Veeco Instruments (now Bruker, USA) using MESP-LC cantilevers (Bruker AFM Probes, USA). The magnetic force microscopy measurements (MFM) were carried out at the room temperature on the polished samples. The measurements are executed by two-pass methods. In the first pass the topography is determined in the contact mode. In the second pass the cantilever is lifted to a selected height for each scan line (or after topography measurement), and scanned using the stored topography (without the feedback). During the second pass method the cantilever is affected by long-range magnetic force. Both the height image and the magnetic image are obtained simultaneously within one method.

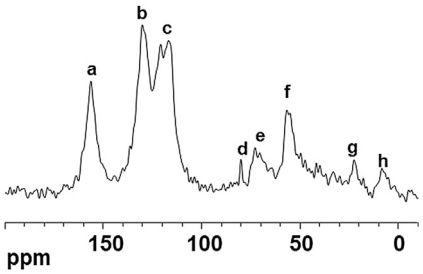

Fig. 1. ^{13}C CP/MAS NMR spectrum of organo-inorganic $PFRSiO_2$ hybrid system.

Complex permeability spectra were measured by an impedance analyzer (HP4194A) from 1 kHz to 40 MHz with the contact electrodes in two-terminal connection configuration. The AC hysteresis loops were measured using MATS-2010SA. All measurements were carried out at room temperature. Total core losses P were calculated directly from the measured hysteresis loops. Electrical resistivity was measured on the cylindrical shaped samples determined by Teraohmmeter–Picoampermeter Sefelec M1501P.

3. Results and discussions

3.1. NMR analysis

The solid-state NMR spectroscopy was used to study the structure and ordering of the prepared hybrid organic–inorganic $PFRSiO_2$ resin. At first, we have performed the characterization of the resin by ^{13}C CP/MAS NMR technique and the resulting spectrum is shown in Fig. 1. All peaks of the resulted material labeled in ^{13}C CP/MAS NMR have been assigned using liquid ^{13}C NMR techniques and literature data [27]. The ^{13}C CP/MAS NMR spectra of the prepared $PFRSiO_2$ sample fit well to the structure of building units used. The NMR data illustrated in Fig. 1 show the spectrum containing three different parts, namely, the region 100–170 ppm corresponding to the aromatic part of $PFRSiO_2$ polymer (signals a–c), the region between 80 and 30 ppm reflecting the aliphatic carbons of $PFRSiO_2$ polymer (signals d–f), and the low-frequency region 0–20 ppm corresponding to the carbon atoms from GLYMO chemically bonded to the silicon atoms (signals g, h). Specifically, the peak at 156 ppm (a) was assigned to the phenoxy carbons, the signal at 130 ppm (b) corresponds to o-, m-, p substituted carbons and the peaks at 121 ppm and 116 ppm labeled as (c) were assigned to unsubstituted carbon atoms of the aromatic rings. The peak at 82 ppm (d) confirms the presence of the methylene groups from polyoxymethylene oligomers (i.e. the residues of formaldehyde after polycondensation reaction) [28]. The signals in the range 65–75 ppm marked as (e) were ascribed to dimethylene ether bridges ($-CH_2-O-CH_2-$) and methylene groups, which are adjacent to the oxygen atoms from GLYMO. The broad signal between 27 and 62 ppm (f) contains the signals of methylol groups and all types of the methylene bridges. The peaks (g) and (h) at resonances 22 ppm and 8 ppm, respectively, then reflect the methylene groups near silicon atoms.

Table 1
The curing schedule used for $PFRSiO_2$.

T °C	40	50	60	70	80	90	100	110	120	130	140	150	160	170	180	190	200
Time/h	1	1	1	1	2	2	0.5	0.5	0.5	0.5	0.5	0.5	0.5	0.5	0.5	0.5	0.5

For a more detailed description of the prepared organic–inorganic polymeric system, the inorganic part was investigated by ^{29}Si CP/MAS NMR spectroscopy. Predominantly, the quantitative analysis of the recorded ^{29}Si CP/MAS NMR spectrum (Fig. 2) allowed calculation of the polycondensation degree q_i:

$$q_i = \left(\sum_{n=1}^{3} nT^n * \frac{1}{3}\right) + \left(\sum_{n=1}^{4} nQ^n * \frac{1}{4}\right)$$

where T^n and Q^n are the mole fractions of each corresponding siloxane structure unit arising from from GLYMO and TEOS, respectively, and n denotes the total number of silicon atoms surrounding the central $-CH_2-SiO_3$ (from GLYMO) and SiO_4 (from TEOS) units. The mole fractions of siloxane units were obtained from the ^{29}Si CP/MAS NMR spectrum by deconvolution procedures. Reliability of the applied procedure was verified by the measurement of the single-pulse ^{29}Si MAS NMR spectrum (not shown here). The pattern of both spectra was nearly identical with the exception of high noise in ^{29}Si MAS NMR spectrum. The determined chemical shifts of the signals at −57, −66, −101 and −111 ppm reflecting T^2, T^3, Q^3 and Q^4 structure units, respectively, are in good agreement with the literature data [29,30]. The obtained results thus suggest that T^3 units arising from GLYMO are dominant in the overall polymeric structure of $PFRSiO_2$ with a minor contribution of the other units (T^2, Q^3 and Q^4) arising from GLYMO and TEOS. Besides, the high polycondensation degree (q_i = 0.93) and the resulting spectrum also confirm almost fully condensed polysiloxane network.

3.2. TG, DSC, FTIR analysis

Fig. 3 illustrates the thermal behavior of the native PFR and the hybrid $PFRSiO_2$ resins under the thermal treatment. The first transition temperature is evident in the region from 100 °C to 200 °C. The main crosslinking reaction, which is responsible for building up the polymeric network, takes place exactly in this temperature range. A lot of volatile by-products are evolved during this stage of the thermal treatment, which generically cause technologically undesirable effects such as a creation of pores, cracks and foam on the surface. The dimensional and shape instability caused by a rapid evolution of water and other volatile by-products have been described in detail in several previous studies [6,11,31,32]. It is evident from the comparison of TG curves for the pure PFR and the hybrid $PFRSiO_2$ resins that the suppression and retardation of the crosslinking reaction occurs in the $PFRSiO_2$ resin above 175 °C. Hence, it follows that the chemical incorporation of silica leads to a more gradual release of water and thus, the silica prevents the formation of micro- and macrovoids in the FeSi/$PFRSiO_2$ samples. A presence of silica was also verified from a comparison of the charge yield, which is 77% for the hybrid $PFRSiO_2$ resin but 91% for the native PFR resin. The second temperature region from 200 °C to 500 °C corresponds to a local plateau in the relevant TG curves and characterizes a thermal stability of both

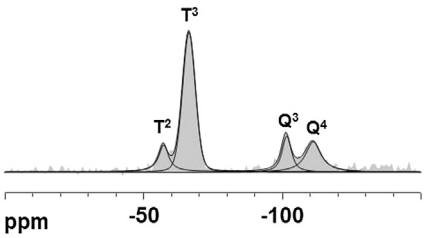

Fig. 2. ^{29}Si CP/MAS NMR spectrum of the hybrid organo-inorganic $PFRSiO_2$ and the deconvolution on individual spectral components. The original spectrum is reflected by gray areas.

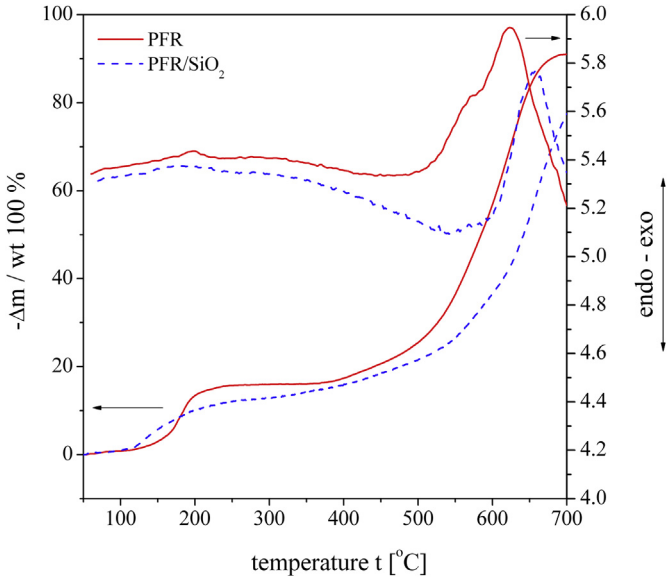

Fig. 3. TG and DSC curves of the pure PFR resin and the hybrid $PFRSiO_2$ resin. TG (DSC) curves are scaled to the left (right) axis.

kinds of resins. A larger thermal stability above 175 °C can be attributed to the hybrid $PFRSiO_2$ resin due to the lower mass loss in this temperature region. The third region from 500 °C to 700 °C relates to the pyrolysis and the overall collapse of the polymeric structure. A presence of silica in the polymeric network of $PFRSiO_2$ reduces the production of combustible gases and moreover, it also decreases and shifts an exothermal peak of the pyrolysis reaction to higher temperatures.

The representative FTIR spectra of the hybrid $PFRSiO_2$ resin in the uncured as well as cured form are depicted in Fig. 4 along with the FTIR spectrum of SiO_2. The characteristic vibrations for silica are well known and they were described in several previous works [33,34]. The most important signals of silica can be attributed to

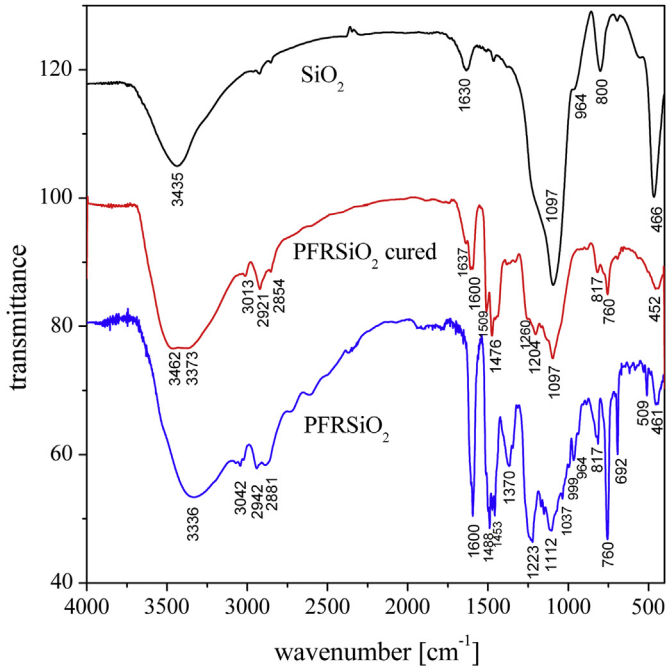

Fig. 4. FTIR spectra of SiO_2 and the hybrid $PFRSiO_2$ resin in the uncured and cured form.

Table 2
Characteristic infrared absorptions frequencies for $PFRSiO_2$ in cured and uncured form.

Band position/cm^{-1}				Assignments	Ref.
Literature data wavenumber	PFR/SiO_2 uncured	PFR/SiO_2 cured	SiO_2		
3400	3336	3462, 3373		Phenolic, Alcoholic O–H stretch	[35]
3026	3042	3013		C–H unsaturated stretch	[35]
2925	2942	2921		In phase stretching vibration of $-CH_2-$ alkane	[35]
2850	2881	2854	–	Out of phase stretching vibration of $-CH_2-$ alkene	[35]
1630	–	–	1630	OH bending vibration of adsorbed molecular water, overtone SiO_2 vibration	[33]
1633	–	1637	–	Aromatic C=C ring stretch	[35]
1626, 1610, 1600	1600	1608, 1596	–	Aromatic C=C ring stretch	[35,36]
1504	–	1509	–	Aromatic C=C ring stretch	[35]
1480	1488	1476		CH aliphatic	[35]
1450	1453	–	–	C=C benzene ring obscured by $-CH_2-$ methylene bridge	[35]
1380	1370	–	–	OH in plane	[35]
1275–1245	Overlapped	1260	–	Si–CH_3 in polysiloxanes	[38]
860–750					
1237	1223	1204		Asymmetric stretch of phenolic C–C–OH	[35]
1100	1112	–		Asymmetric stretching C–O–C of aliphatic ether	[35]
1200		1204		Alkyl–phenol C–O stretch	[34]
1092	Overlapped	1907	1097	Asymmetric and symmetric vibrations of Si–O–Si	[34]
1000	1037, 999	–	–	Aliphatic hydroxyl 1,2,4 substituted benzene ring	[35]
972	964	–	964	Si–O–($H\cdots H_2O$) bending vibration	[33]
790–820	817	817	800	The ring structure of SiO_4 tetrahedra	[37]
760	760	760	–	CH out of plane, orthosubstituted	[35]

asymmetric and symmetric vibrations of Si–O–Si bonds located at 1097 cm^{-1} and 800 cm^{-1}, respectively. The signal at 964 cm^{-1} can be assigned to the Si–O–($H\cdots H_2O$) bending vibration and the band at 1630 cm^{-1} can be attributed to the overtone SiO_2 vibration and stretching vibration of OH of the adsorbed molecular water. The most robust bands represent asymmetric and symmetric vibrations of Si–O–Si bonds, which can be clearly identified in the synthesized $PFRSiO_2$ resin. An assignment of other characteristic peaks of the prepared $PFRSiO_2$ polymer was performed on the basis of the previously published literature (see Table 2), which has precisely described FTIR spectra of the phenol-formaldehyde prepolymer in relation with the spectra of the pure phenol and formaldehyde. A significant broad peak at 3336 cm^{-1} in the uncured $PFRSiO_2$ prepolymer (blue curve (in the web version)) corresponds to phenolic, alcoholic O–H stretching vibrations and the residual water as proposed also by NMR analysis (Scheme 3). After the crosslinking of resin, the narrowing of this band was observed together with a slight shift of its location to higher wavenumbers (see the red curve for the cured $PFRSiO_2$ prepolymer). The gradual heating up to 200 °C, which is closely related to the elimination of water and a creation of the stable polymeric net through the methylene bridges formed from the formaldehyde after the polycondensation reaction, is also evident from the change in the intensities of alkanes and alkenes stretching vibrations. The main differences between FTIR spectra of the uncured and cured $PFRSiO_2$ resins are in the loss of OH bands after the heat treatment, which is consistent with the vanishing of peaks from OH vibrations at 1370 cm^{-1} related to the residual water and at 964 cm^{-1} corresponding to dehydroxylation of the incorporated SiO_2 nanoparticles. The characteristic signals inherent to the methylene bridges C–H are evident in both forms of

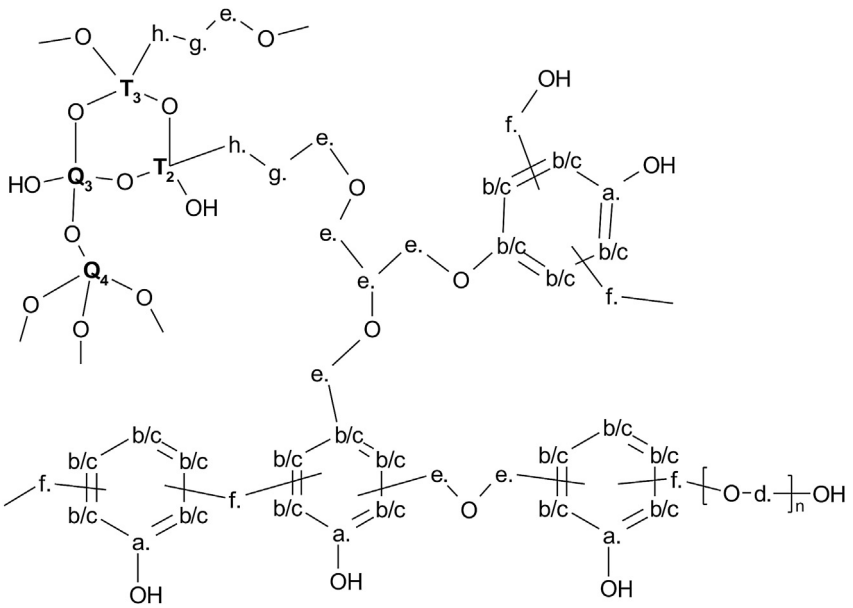

Scheme 3. The proposed structure of the hybrid organic–inorganic resin $PFRSiO_2$ in the uncured form, which is schematically build up from the units a–f, Q^n and T^n as described by our analysis of ^{13}C and ^{29}Si CP/MAS spectra.

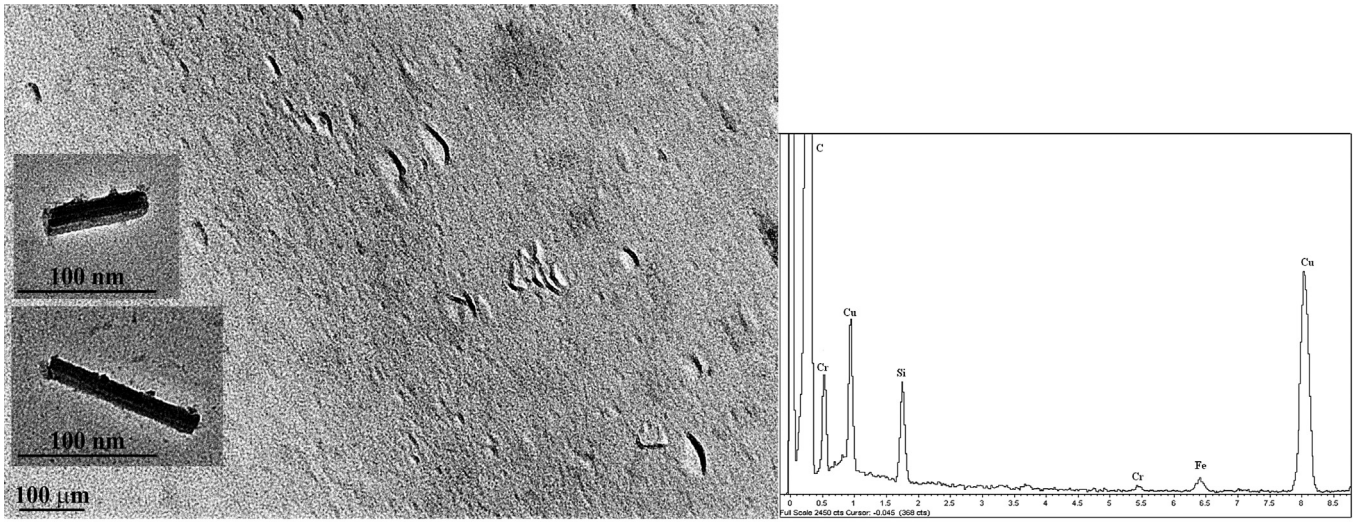

Fig. 5. TEM image of the hybrid polymer PFRSiO$_2$, which confirms a presence of SiO$_2$ nanorods intercalated in the polymer matrix. EDX analysis corresponds to the SiO$_2$ nanorod illustrated in the lower zoom.

the hybrid resin (in the uncured form at 1488 cm^{-1} and in the cured form at 1476 cm^{-1}). However, the methylether bridge C–O–C band at 1112 cm^{-1} manifest itself more clearly in the uncured form of PFRSiO$_2$ resin. Note that this signal strongly overlaps in the cured form of PFRSiO$_2$ resin with intensive signal of the asymmetric stretching vibration Si–O–Si of silica. The strong signal of the methylether bridges is in a good agreement with the structure suggested by ^{13}C and ^{29}Si NMR analysis of the hybrid PFRSiO$_2$ prepolymer. The peak at 1260 cm^{-1} in the cured form of resin confirms the organosilicon group Si–CH$_3$. Unfortunately, the precise identification of infrared bands in polysiloxane parts of the uncured resin is much more difficult because of a substantial overlap of these weak signals with intensive signals of silica.

3.3. TEM, SEM, AFM characterization

TEM provides further insights into the morphology, substructure and size of SiO$_2$ nanoparticles synthesized in situ with the PFR polymer matrix (Fig. 5). The presence of SiO$_2$ nanoparticles anchored in the polymer matrix was confirmed not only by TEM, but also by EDX analysis. EDX analysis indicates a presence of C, Si and O peaks in addition to C and Cu peaks from TEM grid and Fe peak from TEM holder. The outcomes of our measurements have confirmed that SiO$_2$ particles have preferably nanorod shape in average of 150 nm length and of 10 nm diameter. It is worthy to notice that the chemical incorporation of SiO$_2$ nanorods into the PFR resin prevents a high tendency of the silica to form agglomerates, which would otherwise naturally occur on behalf of a different polarity of the hydrophilic silica particles and the hydrophobic PFR polymer matrix. The chemical incorporation of SiO$_2$ into the PFR polymer matrix is also responsible for better thermal properties described in the previous Subsecection 3.2, as well as, the significantly better mechanical properties of the prepared microcomposite samples FeSi/PFRSiO$_2$ to be described in a more detail in the following Subsection 3.4.

The final microcomposite samples FeSi/PFRSiO$_2$ were investigated by SEM (Figs. 6–10). First, the typical spherical morphology of the original commercial FeSi powder is shown in Fig. 6. The

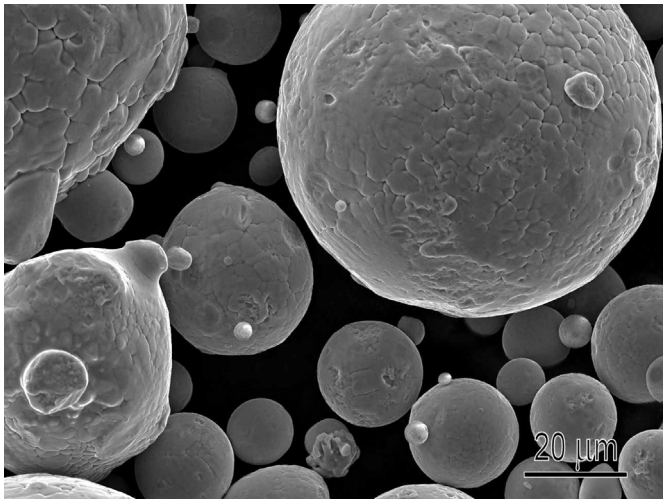

Fig. 6. SEM image of the commercial FeSi spherical powder produced by Hoganas corporation [10].

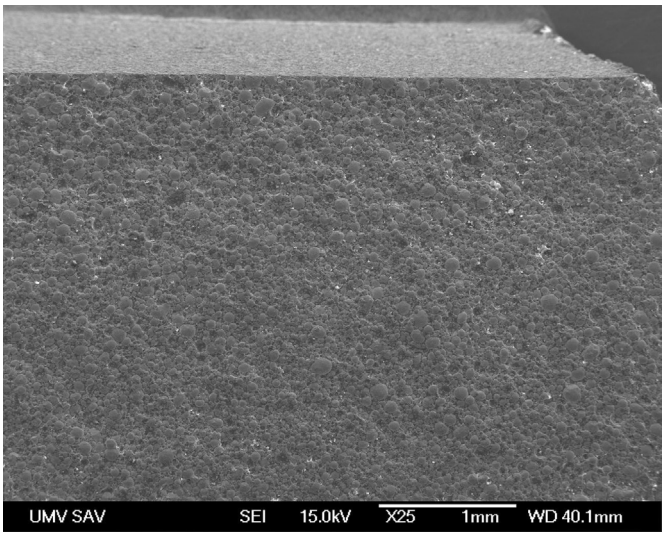

Fig. 7. SEM image displaying the macrostructure of the fractured surface of the prism-shaped sample.

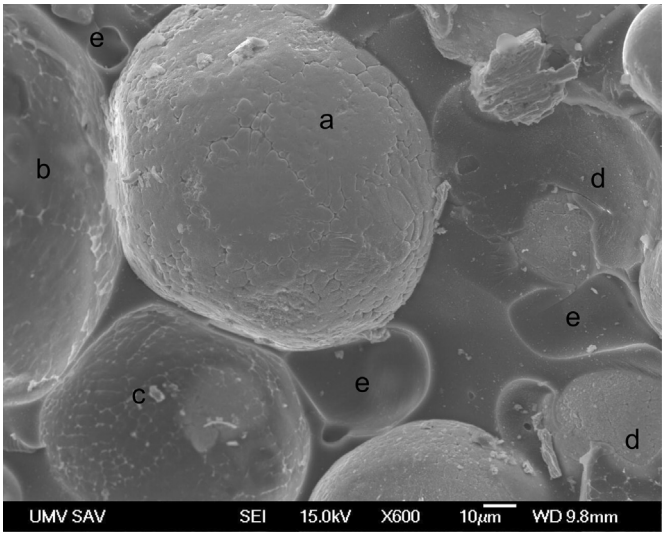

Fig. 8. SEM image of the fractured surface: a) the uncovered FeSi particle, b) the callosity of resin after falling out of one spherical FeSi particle, c) the completely covered FeSi particle by $PFRSiO_2$, d) disrupted coating after fracture, e) pores.

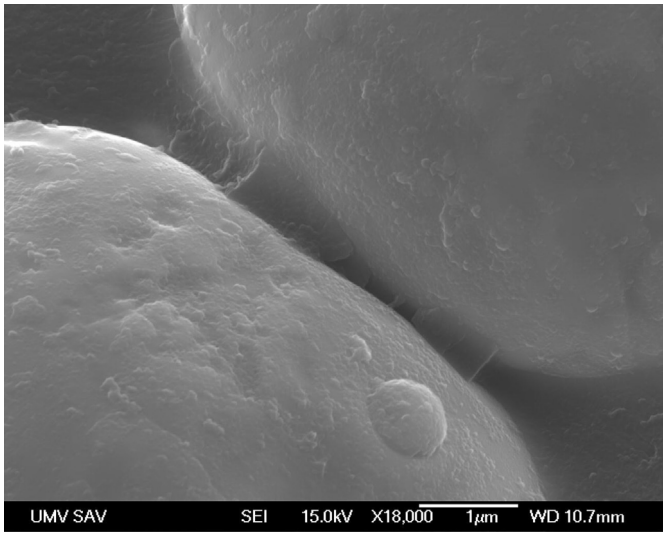

Fig. 10. SEM image of two FeSi particles coated and sticked together by $PFRSiO_2$ inside $FeSi/PFRSiO_2$ sample.

fracture surface of the prism-shaped sample shows no defects and/or structural imperfections in the prepared composite neither before nor after curing, which is highly desirable from the technological point of view (Fig. 7). To the best of our knowledge, phenolic resin without any modification causes a shape and dimensional instability of the final samples because of foaming of resin on the surface and evolving of volatile gas products from the polymer. A more detailed SEM image on the microstructure of the fractured $FeSi/PFRSiO_2$ surface is depicted in Fig. 8. It is quite apparent from this figure that the hybrid coating $PFRSiO_2$ has a tendency to cover the surface of FeSi microparticles completely and quite uniformly. For the better understanding of composition inside of the microcomposite $FeSi/PFRSiO_2$, the same places are marked as follows: a) uncovered FeSi particles after the fracture of the sample – the rest shell of resin stays on the opposite fracture part, b) the callosity of resin after falling out of one spherical FeSi particle, c) the completely covered FeSi particle by the hybrid resin $PFRSiO_2$, d) disrupted coating after fracture, e) pores. Another important observation can be made from the polished surface of the $FeSi/PFRSiO_2$ samples (Fig. 9), which implies a quite uniform distribution of the polymeric network $PFRSiO_2$ in between the FeSi particles. A perfect coating of the FeSi particles is also confirmed by an enormous increase of the specific electric resistivity, which is several orders of magnitude greater than that of the relevant literature data for the compacted FeSi powder (see Table 3). To illustrate a complete covering of FeSi particles by the polymeric shell $PFRSiO_2$, Fig. 10 displays in the enlarged scale how two FeSi particles are held together by means of $PFRSiO_2$ coating. The fact that the hybrid $PFRSiO_2$ resin indeed acts as a plausible inter-particle spacer was also verified by the combination of AFM and MFM techniques (Fig. 11). The domain structure detected in MFM mode will be comprehensively discussed in the Subseection 3.4. The polished surface area of the final $FeSi/PFRSiO_2$ sample with dimension of 6×6 μm provides additional information about the inter-particle spacer, which represents the hybrid resin between FeSi particles (zoom in Fig. 11). Apparently, one cannot detect in Fig. 11 any imperfection or exfoliation of electro-insulating layer in the final $FeSi/PFRSiO_2$ sample, which illustrates the typical inter-particle separation between FeSi particles of approximately 1 μm through the relevant AFM-MFM image. The different height between resin and iron in the three-dimensional view was caused by chemical polishing of the sample, since the polishing suspension etches better the surface of iron than the surface of hybrid resin.

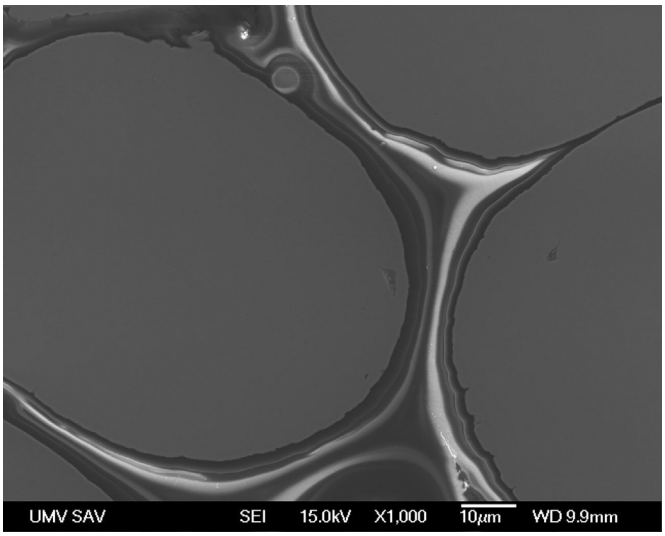

Fig. 9. SEM image of the resin distribution around FeSi particles.

3.4. Mechanical, electrical and magnetic properties

The basic mechanical, electric and magnetic properties of the final composite sample $FeSi/PFRSiO_2$ are compared in Table 3 with the relevant properties of the commercially sintered FeSi sample. It directly follows from this comparison that the density and

Table 3
Mechanical, electric and magnetic properties of the final $FeSi/PFRSiO_2$ samples.

Sample	Density ρ (g cm^3)	Hardness HV 10	Flexural strength (MPa)	Specific resistivity ρ (μΩ m)	Coercitive field H_c (kA m^{-1})
Fe–Si	6.8 [3]	140 [39]	[a]	0.6 [3]	0.02–0.08 [3]
$FeSi/PFRSiO_2$	6.41	140.17 ± 2.48	96.76 ± 2.91	2×10^6	0.1–0.2

[a] Not quoted due to a high plasticity of FeSi powder.

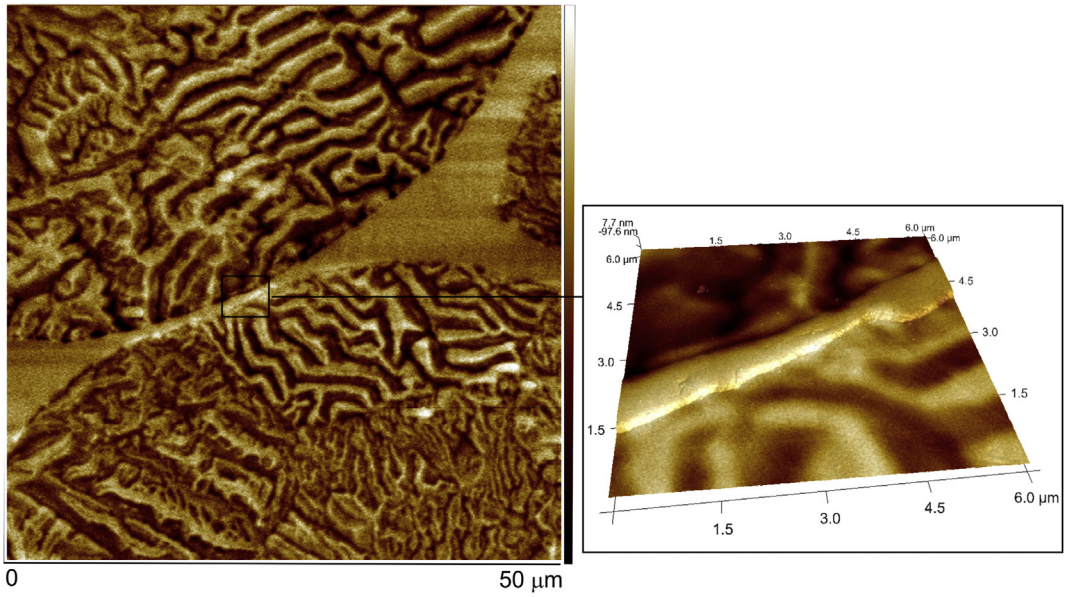

Fig. 11. MFM image of two FeSi particles bonded by $PFRSiO_2$ in FeSi/$PFRSiO_2$ sample.

mechanical hardness of prepared FeSi/$PFRSiO_2$ sample have very similar values as the sintered FeSi powder prepared by the standard PM technologies at relatively high temperature in a hydrogen atmosphere [39]. Moreover, the sufficiently high value of flexural strength demonstrates a reduced brittleness of the composite material that would also suggest an improved handling. A sufficient coating of FeSi particles is evident from a substantial growth of the specific resistivity of FeSi/$PFRSiO_2$ sample, which is seven orders of magnitude greater than that of the sintered FeSi sample and thus evidences an absence of local contacts between FeSi particles in FeSi/$PFRSiO_2$. On the other hand, the coercitive field of the composite FeSi/$PFRSiO_2$ sample remains of the same order of magnitude as the coercitive field of sintered FeSi sample, which evidences that the prepared composite still belongs to SMCs.

A typical cross-section of one FeSi particle is displayed in Fig. 12a as obtained by AFM technique. It can be easily seen from this figure that the selected particle consists of several grains, whereas the respective grain boundaries are well visible as thin lines. The domain structure of the same area is visualized in Fig. 12b by MFM imaging. It is quite clear from this figure that each grain has its own domain structure consisting of several magnetic domains. Our recent work has confirmed a random crystallographic orientation of individual grains and significant differences in a respective domain structure of the most of ferrite grains when the results obtained from the electron backscattering diffraction (EBSD) technique are combined with the relevant MFM analysis [41]. The domain structure with wide lamellar domains (of about 3 µm width) separated by 180 domain walls shows that easy magnetization axes of two grains (depicted in left bottom part of figure) is nearly perpendicular to the surface. Obviously, the easy magnetization axes of the other crystallographic grains largely deviate from the surface direction and hence, one probably detects only branched closure domain structure.

The frequency dependence of the real (μ') and imaginary (μ'') part of initial complex permeability of FeSi/$PFRSiO_2$ composite are displayed in Fig. 13. It can be seen that real μ' part of the

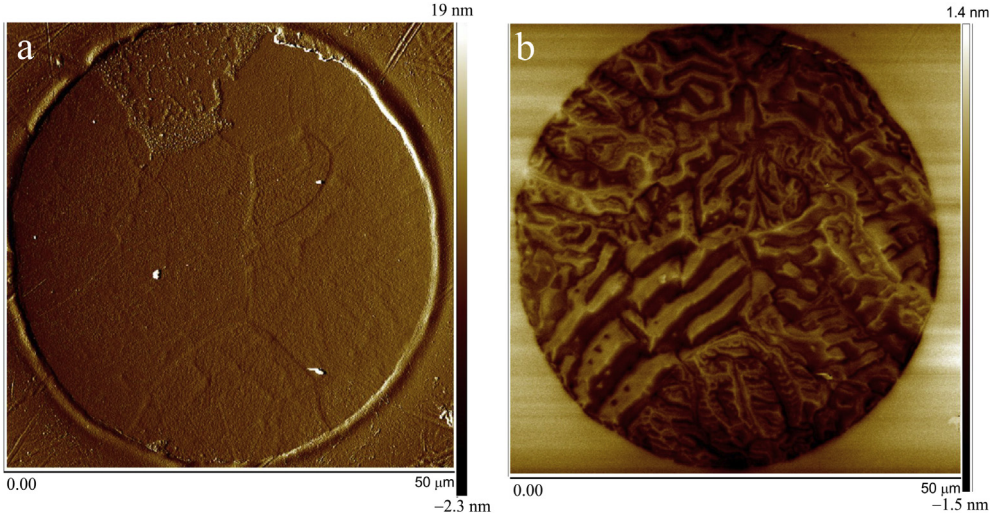

Fig. 12. The a) AFM and b) MFM images of one Fe–Si particle.

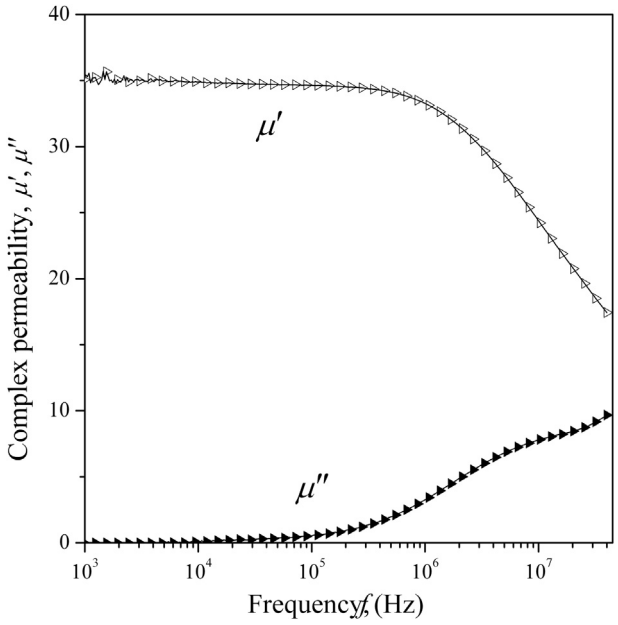

Fig. 13. The real $\mu'$and imaginary μ'' part of the complex permeability μ bulk FeSi/$PFRSiO_2$ composite core (real volume excluding porosity).

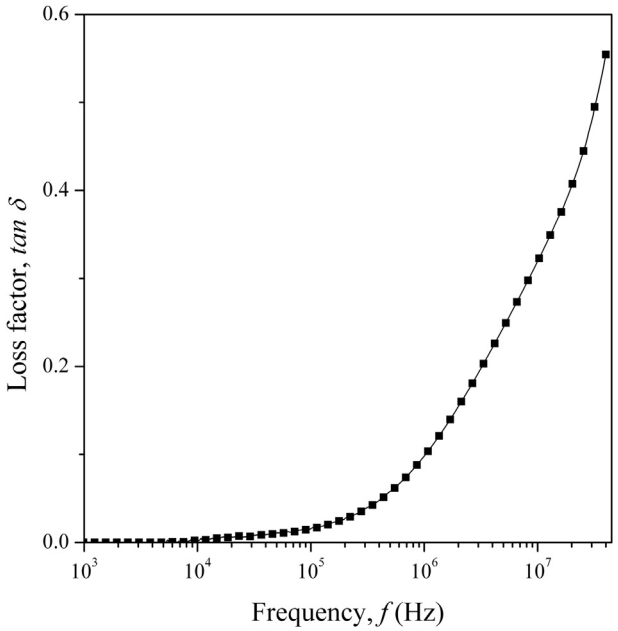

Fig. 14. The loss factor, tan δ of bulk FeSi/$PFRSiO_2$ composite core.

permeability keeps almost constant up to 1 MHz due to a high electric resistivity. The electric resistivity is a significant factor that influences eddy currents closely related to a damping of domain wall motion. A rather large resistivity extends a range of the sizeable real permeability to higher frequencies, where eddy current losses (classical and those due to domain wall motion) dominate the overall power losses [42,43]. It is noteworthy that the real part of permeability strongly depends on the density, number of pores, non-magnetic phase, crystal anisotropy and magnetic anisotropy. Due to the demagnetizing field, the permeability is also related to a density of the core and the shape of magnetic particles. For example, the presence of a non-magnetic material between the magnetic powders acts similarly as an air gap, which is an additional source of demagnetizing field. The frequency dependence of the imaginary part of the complex permeability is in agreement with the real part of the permeability. The imaginary μ'' part of the complex permeability generally reflects the power losses owing to eddy currents and hysteretic response. It can be seen from Fig. 13 that the imaginary μ'' part of the complex permeability increases in a frequency region where the real μ' part of permeability rapidly decreases. However, the relaxation frequency is beyond the technical possibility of our impedance analyzer (40 MHz). Fig. 14 shows the frequency dependence of the loss factor given by tan $\delta = \mu''/\mu'$. The frequency range within the loss factor has a reasonable low value up to 100 kHz.

DC and AC magnetic properties are represented by the hysteresis loops measured up to the maximum induction $B_m = 0.1$ T either at DC or at frequency $f = 62$ kHz, respectively (see Fig. 15). The detected peaks in the permeability as well as the shapes of the hysteresis loops do not change significantly with increasing the frequency up to 100 kHz. The overall hysteresis losses are caused in part by pinning sites of magnetic domains stemming from imperfections of the final composite material and in part by the stresses introduced during the compaction. The energy loss versus frequency dependence shown in Fig. 16 has been measured at the flux density $B_m = 0.1T$. It could be concluded that the absolute value of total core losses at higher frequencies are comparable with commercially produced SMCs described in Ref. [40].

3.5. Final correlations between processing parameters and properties

The sol–gel synthesis of hybrid phenolic resin with chemically incorporated silica nano-particles leads to a creation of SMCs with considerable shape and dimensional stability after thermal curing process. The silica acts as an excellent adsorbent of water evolving during the crosslinking as a volatile by-product and thus, it avoids creation of internal cracks, bubbles and surface bulges. A small amount (about 3 wt%) of the hybrid resin $PFRSiO_2$ is sufficient to provide a thin but structurally perfect electroinsulating layer on a surface of FeSi particles, what consequently ensures exceptionally high value of specific electric resistivity under the simultaneous maintenance of a sufficiently low coercivity and high enough permeability. Among the most important factors that essentially

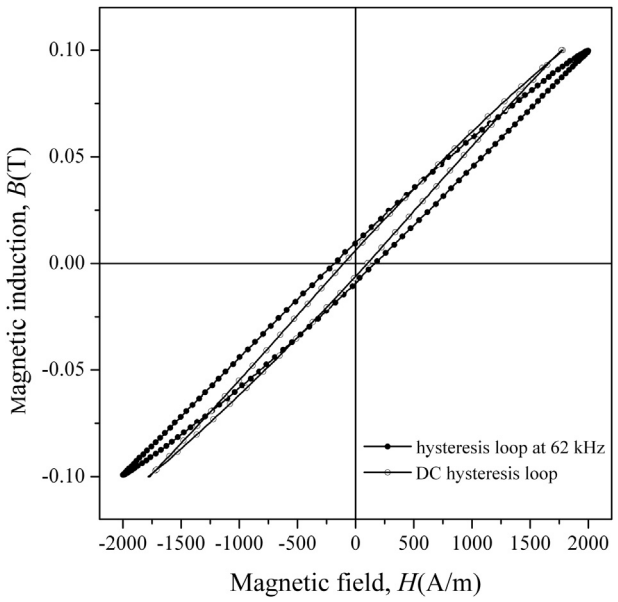

Fig. 15. DC and AC (62 kHz) hysteresis loops of bulk FeSi/$PFRSiO_2$ composite core at $Bm = 0.1$ T.

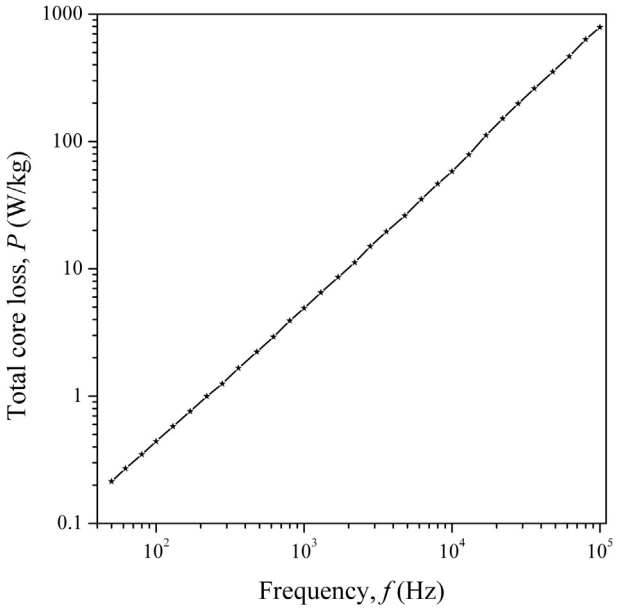

Fig. 16. Frequency dependence of the total core loss for bulk FeSi/PFRSiO$_2$ composite core.

influence the overall properties of the final SMCs one could also mention compressing parameters and curing schedule, which have allowed us to produce under the optimal conditions FeSi/PFRSiO$_2$ samples with nearly equal mechanical hardness and density as that ones of the sintered FeSi products.

4. Conclusions

The novel SMC, which is composed of spherical FeSi powder covered by the phenolic resin chemically modified with silica nano-particles, has been prepared and investigated in detail. The synthesis of hybrid resin has been performed by the modified sol–gel method exploiting two different silanes. The chemically incorporated SiO$_2$ nano-particles are rod-like of the average size of about 100 nm as confirmed by TEM and EDX analyses. The chemical structure of the hybrid resin and also chemical bonding of the silica nano-particles has been confirmed by NMR and FTIR analyses. It was demonstrated that the hybrid inorganic–organic resin PFRSiO$_2$ displays an improved thermal stability up to 550 °C in comparison with the pure PFR, which is of immense practical importance from the technological point of view. The prepared hybrid resin offers a reliable option for being used as an electroinsulating layer, which perfectly covers the surface of FeSi particles and avoids the inter-particle contacts. SEM images have provided us useful information about: i) the size, character of surface and shape of original FeSi particles, ii) the precise covering of spherical FeSi particles by the insulating polymer PFRSiO$_2$, iii) the minimum width of insulating polymeric spacer that still links FeSi particles together. A grain distribution, grain boundaries and magnetic structure has been investigated by AFM-MFM technique. Altogether, it could be concluded that the designed FeSi/PFRSiO$_2$ composite exhibits comparable mechanical properties as the sintered FeSi powder and moreover, FeSi particles are covered just by a relatively small amount of the insulating spacer PFRSiO$_2$ that makes electric and magnetic properties of FeSi/PFRSiO$_2$ quite superior with respect to the sintered FeSi powder. An immense increase in the specific resistivity is consistent with much lower total core losses at medium up to high frequencies without any significant decline in the basic magnetic properties (coercitive field, saturation magnetization) of the underlying FeSi ferromagnetic powder with respect to a small amount of the insulating spacer used. From this perspective, the fabricated material represents quite promising SMC with a remarkable combination of mechanical, electric and magnetic properties for further development.

Acknowledgment

This work was financially supported by Slovak Research and Development Agency under the contract no. APVV-0222-10 and by the project "The progressive technology for preparation of micro-composite materials for electrotechnology", ITMS 26220220105, which is supported by the Operational Program "Research and Development" financed through European Regional Development Fund.

References

[1] J.A. Bas, J.A. Calero, M.J. Dougan, J. Magn. Magn. Mater. 254-255 (2003) 391–398.
[2] H. Shokrollahi, K. Janghorban, J. Mater. Process. Technol. 189 (2007) 1–12.
[3] K. Narasimhan, F. Hanejko, M.L. Marucci, ChemInform, 41, 287. http://www.yunamedia.com/www.hoegtest.com/TechPapersv2/201.pdf.
[4] S. Pelletier, P. Lemieux, L. Azzi, in: Properties and Processing of Improved SMC Materials, of Industrial Materials Institute, and C. Gelinas of QMP, PM2TEC Conference, Montreal, June 2005.
[5] C. Gelinas, Quebec Metal Powders Ltd., P. Viarouge, J. Cros, in: PM2004 World Congress & Exhibition, Electrotechnologies SELEM Inc., Vienna, Austria, October 2004.
[6] M. Strečková, T. Sopčák, Ľ. Medvecký, R. Bureš, M. Fáberová, I. Batko, J. Briančin, Chem. Eng. J. 180 (2012) 343–353.
[7] R. Oriňáková, Surf. Coat. Technol. 162 (2003) 54–60.
[8] H. Brunckova, M. Kabátová, E. Dudrová, Surf. Interface Anal. 42 (2010) 13–20.
[9] M. Kabátová, E. Dudrová, H. Brunckova, Surf. Interface Anal. 45 (2013) 1166–1173.
[10] Höganäs datasheet: http://hoganas.com/Documents/Somaloy%20Broschyrer%20och%20Wear%20Resist/SMC/Spherical_Fe_Si_powders_with_very_low_losses_for_Soft_magnetic_applications_april_2010.pdf.
[11] C. Kaynak, C. Cem Tasan, Eur. Polym. J. 42 (2006) 1908–1921.
[12] P. Kollar, Z. Bircakova, J. Fuzer, R. Bures, M. Faberova, J. Magn. Magn. Mater. 327 (2013) 146–150.
[13] A.H. Taghavaei, H. Shokrollahi, A. Ebrahimi, K. Janghorban, Mater. Chem. Phys. 116 (2009) 247–253.
[14] I. Hemmati, H.R. Madaah Hosseini, A. Kianvash, J. Magn. Magn. Mater. 305 (2006) 147–151.
[15] S. Pelletier, L.P. Lafebvre, C. Gelinass, link: qmp-powders.com/rtecontent/document/RISM_CG97.pdf.
[16] A.H. Taghvaei, H. Shokrollahi, K. Janghorban, J. Magn. Magn. Mater. 321 (2009) 3926–3932.
[17] I. Chicinas, O. Geoffroy, O. Isnard, V. Pop, J. Magn. Magn. Mater. 310 (2007) 2474–2476.
[18] G. Hernandez-Padron, F. Rojas, M. Garcia-Gardun, M.A. Canseco, V.M. Castano, Mater. Sci. Eng. A 355 (2003) 338–347.
[19] I. Hasegawa, Y. Fukuda, M. Kajiwara, J. Eur. Ceram. Soc. 17 (1997) 1467–1473.
[20] X. Zhang, L. Shen, X. Xia, H. Wang, Q. Du, Mater. Chem. Phys. 111 (2008) 368–374.
[21] M. Strečková, J. Füzer, Ľ. Medvecký, R. Bureš, P. Kollár, M. Fáberová, V. Girman, Bull. Mater. Sci. 37 (2014) 167–177.
[22] Y. Xie, C. Callum, A.S. Hill, Z. Xiao, H. Militz, C. Mai, Compos. Part A 41 (2010) 806–819.
[23] M. Strečková, Ľ. Medvecký, J. Füzer, P. Kollár, R. Bureš, M. Fáberová, Mater. Lett. 101 (2013) 37–40.
[24] A.M. Kawamoto, L.C. Pardini, M.F. Diniz, V.L. Lourenco, M.F.K. Takahashi, J. Aerosp. Technol. Manag. 2 (2010) 169–182.
[25] C.L. Chiang, C.C.M. Ma, D.L. Wu, H.C. Kuan, J. Polym, Sci. Part A Polym. Chem. 41 (2003) 905–913.
[26] J. Brus, Solid State Nucl. Magn. Reson. 16 (2000) 151–160.
[27] R. Rego, P.J. Adriaensens, R.A. Carleer, J.M. Gelan, Polymer 45 (2004) 33–38.
[28] A.J.J. de Breet, W. Dankelman, W.G.B. Huysmans, J. de Wit, Angew. Makromol. Chem. 62 (1977) 7–31.
[29] J. Brus, M. Spirkova, D. Hlavata, A. Strachota, Macromolecules 37 (2004) 1346–1357.
[30] J. Brus, J. Dybal, Polymer 41 (2000) 5269–5282.
[31] Y. Chen, Z. Chen, S. Xiao, H. Liu, Thermochim. Acta 476 (2008) 39–43.
[32] Y. Abou Msallem, F. Jacquemin, N. Boyard, A. Poitou, D. Delaunay, S. Chatel, Compos. Part A 41 (2010) 108–115.
[33] L.P. Singh, S.K. Bhattacharyya, G. Mishra, S. Ahalawat, Appl. Nanosci. 1 (2011) 117–122.

[34] T.M.H. Costa, M.R. Gallas, E.V. Benvenutti, J.A.H. da Jornada, J. Non-Cryst Solids 220 (1997) 195–201.
[35] I. Poljansek, M. Krajnc, Acta. Chim. Slov. 52 (2005) 238–244.
[36] M. Křístková, P. Filip, Z. Weiss, R. Peter, Polym. Degrad. Stab. 84 (2004) 49–60.
[37] T. Periadurai, C.T. Vijayakumar, M. Balasubramanian, J. Anal. Appl. Pyrol. 89 (2010) 244–249.
[38] Philip J. Launer, Laboratory for Materials, Inc. Burnt Hills, New York 12027.
[39] GKN Sinter Metals company, link of datasheet: http://www.gkn.com/sintermetals/capabilities/soft-magnetic-pm/Documents/GKN%20PM%20Soft%20Magnetic%20Materials.pdf.
[40] Högänes Insulated Composites Characteristic and Electromagnetic Application Guidelines, http://www.gkn.com/hoeganaes/media/Brochures%20Library/Products/Magnetics/AncorLam®.pdf.
[41] M. Strečková, M. Baťková, I. Baťko, H. Hadraba, R. Bureš, Acta Phys. Pol. A 125 (3) (2014).
[42] A.H. Taghvaei, A. Ebrahimi, M. Ghaffari, K. Janghorban, J. Magn. Magn. Mater. 323 (2011) 149–155.
[43] S. Wu, A. Sun, F. Zhai, J. Wang, Q. Zhang, W. Xu, P. Logan, A. Volinsky, J. Magn. Magn. Mater. 324 (2012) 818–822.